12-1-2012

Wavelength-Dependent Absorption in Structurally Tailored Randomly Branched Vertical Arrays of InSb Nanowires

Asaduzzaman Mohammad
Purdue University, Birck Nanotechnology Center, mohammad@purdue.edu

Suprem R. Das
Purdue University, Birck Nanotechnology Center, srdas@purdue.edu

Mohammad R. Khan
Purdue University, khan23@purdue.edu

Muhammad A. Alam
Purdue University, alam@purdue.edu

David B. Janes
Purdue University, Bick Nanotechnology Center, david.b.janes.1@purdue.edu

NANO LETTERS

Letter

pubs.acs.org/NanoLett

Wavelength-Dependent Absorption in Structurally Tailored Randomly Branched Vertical Arrays of InSb Nanowires

Asaduzzaman Mohammad,[†,§,∥] Suprem R. Das,[‡,§,∥] M. Ryyan Khan,[†,∥] Muhammad A. Alam,*[,†] and David B. Janes*[,†,§]

[†]School of Electrical and Computer Engineering, Purdue University, West Lafayette, Indiana 47907, United States

[‡]Department of Physics, Purdue University, West Lafayette, Indiana 47907, United States

[§]Birck Nanotechnology Center, Purdue University, West Lafayette, Indiana 47907, United States

Supporting Information

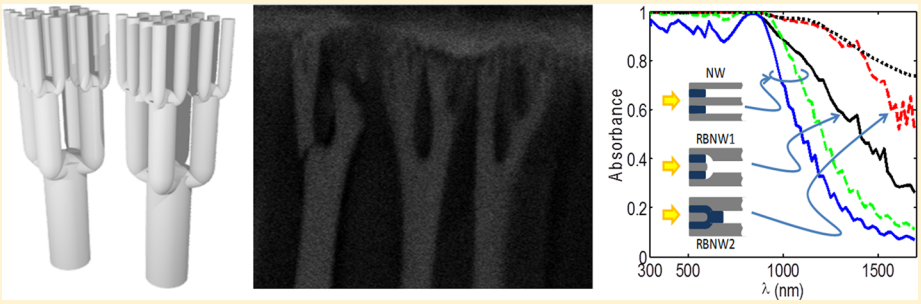

ABSTRACT: Arrays of semiconductor nanowires are of potential interest for applications including photovoltaic devices and IR detectors/imagers. While nominally uniform arrays have typically been studied, arrays containing nanowires with multiple diameters and/or random distributions of diameters could allow tailoring of the photonic properties of the arrays. In this Letter, we demonstrate the growth and optical properties of randomly branched InSb nanowire arrays. The structure mentioned can be approximated as three vertically stacked regions, with average diameters of 20, 100, and 150 nm within the respective layers. Reflectance and transmittance measurements on structures with different average nanowire lengths have been performed over the wavelength range of 300−2000 nm, and absorbance has been calculated from these measurements. The structures show low reflectance over the visible and IR regions and wavelength-dependent absorbance in the IR region. A model considering the diameter-dependent photonic coupling (at a given wavelength) and random distribution of nanowire diameters within the regions has been developed. The diameter-dependent photonic coupling results in a roll-off in the absorbance spectra at wavelengths well below the bulk cutoff of ∼7 μm, and randomness is observed to broaden the absorbance response. Varying the average diameters would allow tailoring of the wavelength dependent absorption within various layers, which could be employed in photovoltaic devices or wavelength-dependent IR imagers.

KEYWORDS: *InSb branched nanowire arrays, IR detectors, nanowires wave-guiding, antireflecting surface, wavelength-selective absorption, structurally tailored photonic effect*

The interaction of light with periodically modulated solid-state nanosystems constitutes the platform for many interesting phenomena in modern optics and metamaterials.[1,2] One system of particular interest for photovoltaic and detector/imager devices involves semiconductor nanostructures (nanowires/nanoclusters), which can effectively absorb light with energies above the local bandgap and yield a photocurrent associated with separating the generated electron−hole pairs. Several groups have investigated aligned arrays of semiconductor nanowires as potential structures of interest for these applications[3−5] (see Figure 1b). There are several physical effects that can be attributed to the use of aligned nanowires. Within a vertically aligned array of nanowires, it is possible to decouple the two fundamental length scales for photovoltaic devices, namely the absorption length (axial in a nanowire array) and the minority carrier diffusion length (radial).[6] At very small diameters, it is also possible to increase the bandgap energy (with respect to the bulk value) via electronic size quantization.[7]

While the interface between air and an array of nanowires provides lower optical reflectance than an air/bulk interface of the same semiconductor, several groups have further reduced surface reflection in structures with tapered or stepped transitions along the length of the nanowire, as shown in Figure 1c. Reported structures include dual-diameter nanopillars (DNPLs),[8] nanoneedles (NNs),[9] and nanoholes (NHs).[10] A DNPL array provides a stepped change between

Received: July 28, 2012
Revised: October 23, 2012
Published: November 6, 2012

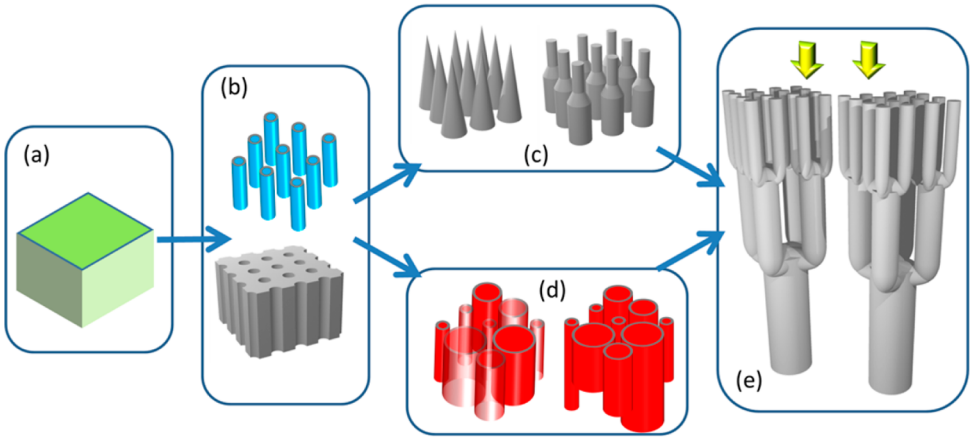

Figure 1. Schematic of various nanostructure arrays being studied for photonic or photovoltaic applications. In contrast to bulk films (a), arrays of nanopores or nanowires (uniform (b) and tapered/dual diameter (c)) can provide wavelength properties associated with size-dependent photonic coupling, resulting in reduced reflection and enhanced absorption. Randomness in diameter within the arrays allows tailoring of the absorption (d) with wavelength. This study investigates hierarchical, branched nanowire structures (e), which can allow tuning of the wavelength-dependent absorption within the various regions.

a low-fill factor top layer and a high-fill factor bottom layer, which provides broadband absorption close to unity in 300−900 nm regime.[8] Conical nanoneedles (NN) provide a tapered change in the fill factor, resulting in a very low reflectance.[9] The lower reflectance is typically attributed to the graded dielectric transition and paves the way for allowing a higher fraction of the incident light to be absorbed.

Many prior nanowire array studies have considered dielectric properties associated with the nonunity filling ratio and/or graded/stepped transition, which can generally be understood in terms of an effective media analysis.[3,9] However, one would expect photonic effects, e.g., the coupling between photons and the nanowires to depend on the ratio between the photon wavelength and the local nanowire diameter. Hu et al.[3] theoretically analyzed the reflectance and absorption of a silicon nanowire array as a function of the diameter, length, and filling ratio of individual nanowire arrays. This study concluded that in the short wavelength regime (<413 nm) the overall fraction of incident light absorbed within the array is much higher than that of a thin film structure, due to decreased reflection. The absorption in the longer wavelength region (413−1127 nm) is suppressed but can be improved with NW length, filling ratio, and/or by introducing light trapping mechanisms.[3]

A second trend in vertically oriented NW involves increasing the diameter distribution, so that a broadband absorption is possible. While highly ordered structures can provide relatively sharp resonances, structures with disorder such as distributions in diameters or lengths, as in Figure 1d, can yield high broadband absorption or wide-angle collection of light.[11] Random NW arrays can provide significant diffused reflectance (in contrast to the specular reflectance in case of a periodic array) arising from strong multiple optical scattering events and can lead to additional light trapping.[11−16] Unfortunately, while the randomness in diameter allows broadband absorption, it is counterbalanced by reduced absorption due to high reflectance of larger diameter NWs.

In this paper, we offer a third possibility to show that a hierarchical, vertical stacking of NWs with random diameter distribution (see Figure 1e) can simultaneously maximize absorption and minimize reflection and thereby combine the advantages of the approaches discussed above. To validate the concept, we present a coupled experimental and modeling study on vertically aligned, branched nanowire arrays. In contrast to most prior branched nanowire studies, the current arrays exhibit hierarchical stacking, i.e., the average diameter changing monotonically from layer to layer. The study demonstrates low reflectance (significantly different from that expected for a thin film of comparable thickness) and a unique wavelength-dependent absorption that can be explained on the basis of structurally dependent photonic effects. The experimental results are well fit by a model considering the wavelength-dependent coupling to a given diameter nanowire and the random distribution of diameters within the various regions of the structure.

Vertical arrays of randomly branched, hierarchical NWs of indium antimonide (InSb) were grown by electrodeposition within branched porous anodic alumina (BPAA) membranes. An idealized cross section of the three-layer structure within a single element of the NW array is shown in Figure 2a. In order to demonstrate the broadband absorption in the entire UV−vis range and wavelength selective absorption in near-infrared (NIR) regime, InSb was chosen due to its very low bandgap (0.17 eV direct bandgap at 300 K which is equivalent to a photon wavelength of ∼7.3 μm). Details of the growth process of the random branched NW (RBNW) arrays are provided in the Methods section and the Supporting Information (see S1). Figure 2b shows cross-sectional field emission scanning electron microscope (FESEM) images of a representative area within a RBNW array. Based on the statistical analysis from FESEM images, the average diameters (average spacing) within the three regions are 20 (40) nm, 100 (220) nm, and 150 (440) nm. The RBNW structure (Figure 2b) exhibits randomness in both diameter and segment lengths. Standard deviations of diameters were estimated within each region and will be discussed later. As we will see, this randomness plays a significant role in defining the optical properties of the branched NW. Following an in-situ anneal, the NWs within the arrays were observed to be phase-pure and highly crystalline by transmission electron microscopy (HRTEM) (see Supporting Information S2). The multilayer stack, in general, can be extended to any number for light manipulation.

In order to decouple the effects and properties associated with various layers in the hierarchical RBNW structure, four

dx.doi.org/10.1021/nl302803e | *Nano Lett.* 2012, 12, 6112−6118

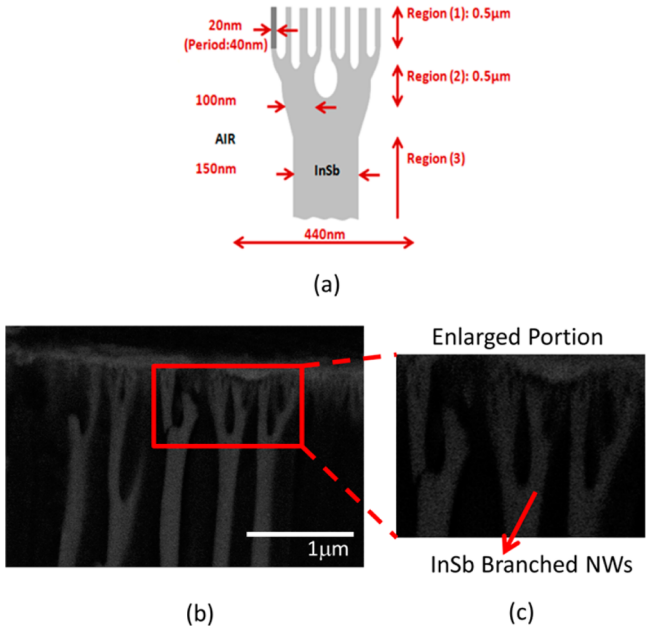

Figure 2. Schematic diagram and cross-sectional FESEM image of a RBNW array after electrodeposition into the nanochannels of a BPAA template: (a) an ideal schematic diagram of the InSb branched nanowire array showing three regions and average diameters/periods within each region; (b) cross-sectional FESEM image of a representative randomly branched nanowire array showing the three layers; (c) zoomed-in section of the array near the top surface.

types of structures (Figure 3a) were characterized. The reference structure (RBNW-ref) consists of a BPAA membrane that is not backfilled with InSb. This structure (RBNW-ref) showed negligible absorption in the spectrum of interest (less than 1% for wavelengths 850 nm and beyond). The second structure (RBNW0) consists of a BPAA membrane backfilled with ~20 μm of InSb followed by a ~ 10 μm etch-back of the alumina to form a free-standing array with a thickness larger than typical absorption lengths (effectively eliminating reflections from alumina surface during reflectance measurements). Finally, RBNW1 (wire length ~800 nm, consisting primarily of regions 1 and 2 (see Figure 2a) and RBNW2 (wire length ~1400 nm, including all three regions) consist of shorter nanowire structures; the alumina membrane was required for structural support and therefore was not etched in these samples. The sample shown in Figure 2b is representative of type RBNW0, prior to back-etching of the alumina.

The reflectance (R) and transmittance (T) of the samples were measured, and the absorbance (A) was calculated from these characteristics. About 1 mm^2 of the "top" surface of each sample (i.e., containing smallest diameter pores/wires) was illuminated at normal incidence (θ = 0°), arranged inside an integrating sphere setup, with the wavelength of the incident light ranging from 300 nm (UV) to 2 μm (NIR to mid-IR) (see Methods section). Uniformity of the nanowire array within the optical spot size is discussed in the Supporting Information (see S3 for details). Figure 3b shows the measured R versus wavelength for the free-standing NW array (RBNW0). For comparison, we plot the R calculated from effective medium approximation[17] using the bulk material parameters of InSb and the fill factors for the different regions (inferred from FESEM). The R of a thin film of equivalent thickness (~800 and ~1400 nm) would be approximately ~47% (UV–vis) and ~37%

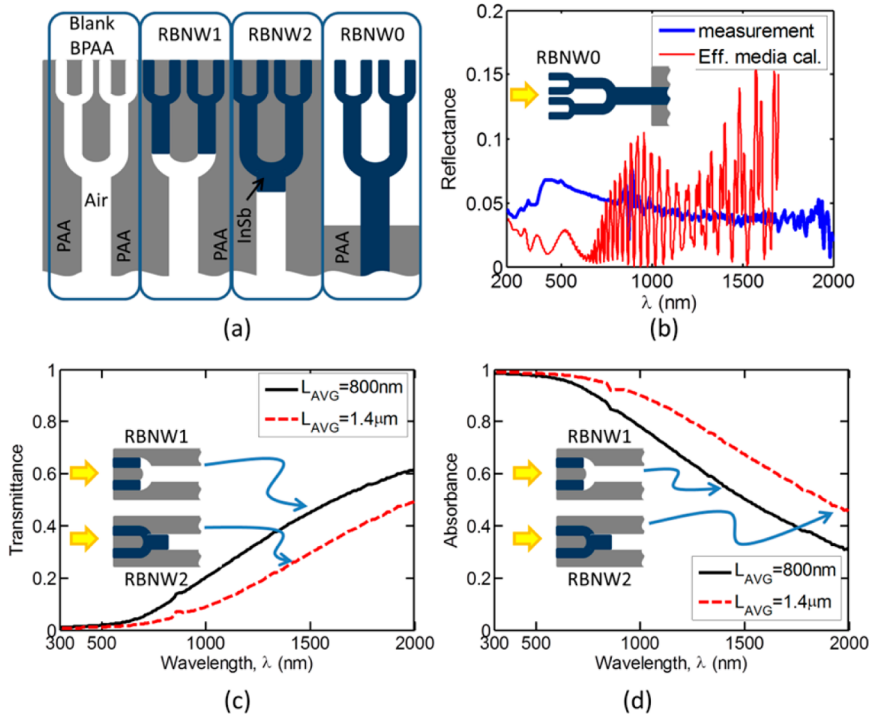

Figure 3. Reflectance, transmittance, and normalized absorbance measurements of vertically aligned branched InSb NWs: (a) simplified cross-sectional schematic of a blank BPAA, BPAA with ~800 nm from top surface filled with InSb (RBNW1), BPAA with ~1.4 μm from top surface filled with InSb (RBNW2), and a schematic of the etched back sample (RBNW0); (b) measured reflectance of RBNW0 and reflectance calculated for same nominal structure from effective medium theory; (c) measured transmittance of RBNW1 (black) and RBNW2 (red); (d) the measured normalized absorbance of RBNW1 (black) and RBNW2 (red), extracted using eq 1.

dx.doi.org/10.1021/nl302803e | Nano Lett. 2012, 12, 6112–6118

(near-IR). While the measured reflectance appears to be well approximated by the effective media approach, we will see later that the approach cannot describe local absorption within and transmission through the photonic nanostructure.

Figure 3c shows the measured T of RBNW1 and RBNW2 in the 300−2000 nm range. The T is small in the lower wavelength range (<700 nm), and it rises linearly for wavelengths >700 nm (RBNW1) and >850 nm (RBNW2), indicating that a broader range of wavelengths is absorbed for samples with significant filling in region 3.

In order to differentiate the effects of absorption and reflection and to allow direct comparison among samples with different R, we define a normalized A, given by

$$A = \frac{1 - R - T}{1 - R} \quad (1)$$

The measured A of RBNW1 and RBNW2 (Figure 3d) shows nearly complete absorption for wavelengths up to ∼700 nm (RBNW1) and ∼850 nm (RBNW2). The absorbance decreases linearly in the NIR regime, with the rate being somewhat faster for the shorter arrays of RBNW. The absorption band can be tuned by designing the RBNW layers with specific average diameters. This broadband and wavelength-dependent absorption along with its tunability in branched NW structure is unique and the key results of our work.

To understand the origin of the wavelength-dependent absorption in such a complex hierarchical RBNW structure and its implication of depth-resolved absorption, we theoretically interpret the T and A spectra associated with the different configurations. The numerical analysis was implemented using the electromagnetic simulator COMSOL RF-module.[18] To replicate the experiments, we use optical properties of InSb and alumina[19] and assume normal incidence of the plane wave. See the Supporting Information, S4, for details.

As we will see below, the characteristic randomness in diameter of RBNW has a significant effect on the broadening of the absorption spectrum, which can be explained neither by a periodic structure nor exclusively by the variation in the lengths of the NWs. In order to understand the effects of this randomness, we employed a model assuming that the diameter has a Gaussian distribution characterized by a mean diameter ($\bar{d}$) and standard deviation (σ). The structures associated with samples RBNW1 and RBNW2 were modeled using two-layer RNW arrays corresponding to regions 2 and 3 in Figure 2. Since NWs with diameters of ∼20 nm do not significantly couple to wavelengths over the measurement range (300−2000 nm), region 1 can be omitted in the optical modeling. This approximation reduces computational burden and simplifies conceptual interpretation of the results. This approach is justified because as we will see later that we can consistently interpret the salient features of the experiments using with the simplified structure.

Analysis of the FESEM images show that the two-step RBNW array structure has $(\bar{d}_a, \sigma_a) \sim (100, 25)$ nm in region 2 and $(\bar{d}_b, \sigma_b) \sim (150, 25)$ nm in region 3. A statistical analysis of the mean diameter and standard deviation of the NWs in regions 2 and 3 is provided in the Supporting Information (see S3). The length of the top region is kept fixed at 700 nm, and the length of the bottom layer is chosen to achieve the same overall length as either RBNW1 or RBNW2. In this model, the NWs are embedded within a thick layer of alumina, to be consistent with the experimental measurements. The modeling details are given in the Supporting Information (see S4).

Figure 4 shows the calculated A versus wavelength for various structures. The A calculated for a spatially uniform thin film with bulk material properties and thickness of 800 nm is also shown for reference (dotted line). To decouple the effects of fluctuation in NW length vs randomness of diameter, a single layer, uniform-diameter (100 nm) NW array (similar to ref 3) is modeled for two different lengths (800 and 1400 nm, solid blue and dashed green curves, respectively). The curves show a relatively sharp cutoff at ∼1000 nm, well below that expected for the bulk thin-film (dotted line) as well those for RBNWs. The fluctuation in NW length therefore cannot explain the broadband absorption observed in experiment.

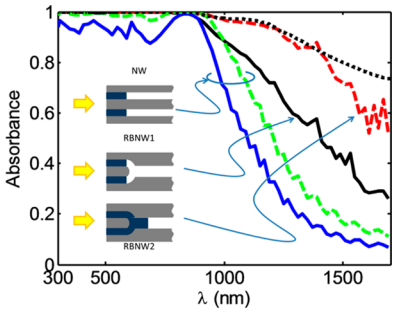

Figure 4. Comparison of numerically determined normalized absorbance for vertically aligned InSb NWs and thin film. Normalized absorbance calculated from model for single-layer NW array with uniform diameter (100 nm) and thicknesses of 800 and 1400 nm (solid blue and dashed green, respectively) and for random diameters for single layer (RBNW1, solid black line) and bilayer (RBNW2, red dashed line). The calculated normalized absorbance for a thin film with bulk properties and thickness of 800 nm (dotted line) is shown for comparison. Structures with uniform diameters have steep decrease in absorbance, corresponding to cutoff wavelength, while structures with randomness in diameter exhibit a more gradual roll-off.

Next we model the responses of the experimental structures RBNW1 (length = 800 nm) and RBNW2 (length = 1400 nm), not as a uniform periodic array but as structures with random diameter distribution in region 2 (for RBNW1) and regions 2 and 3 (for RBNW2). Remarkably, the introduction randomness in diameter immediately broadens the absorption profile. For structures of the same length, the random structures exhibit significant absorption over much broader band, with a more gradual roll-off in the absorption spectrum, in comparison to the uniform array with same length and same mean diameter(s). Consistent with experiments in Figure 3, the structure representing RBNW2 has a more gradual roll-off (in comparison to that of RBNW1), indicative of the two different diameters in the two regions and randomness in both layers. The higher absorption is predominantly due to the bottom layer with higher mean diameter of NWs, which more efficiently couple the longer wavelengths. Based on these simulations, our experimental results are best explained in terms of the wavelength-dependent photonic coupling to the randomly sized nanowires within regions 2 and 3. The roll-off in A reflects the average diameters and characteristic randomness in the branched NW structures. Electronic size quantization effects cannot explain the observed A spectra; even for diameters of 20 nm, the bandgap would be expected to broaden by ∼100 meV (using bulk effective mass for InSb), corresponding to a cutoff wavelength of ∼4.6 μm.

The close agreement between theory and experiment allows us to establish a remarkable feature of the RBNW arrays,

dx.doi.org/10.1021/nl302803e | Nano Lett. 2012, 12, 6112−6118

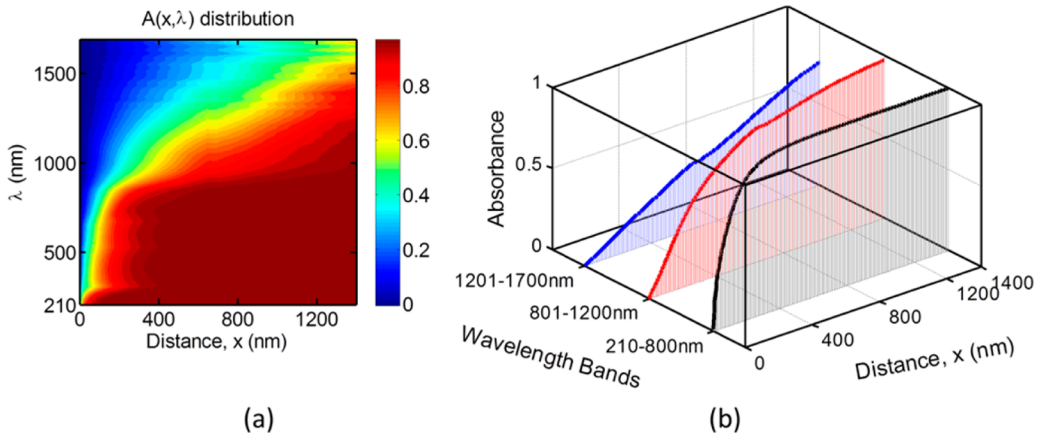

Figure 5. Numerically determined cumulative normalized absorbance of vertically aligned branched InSb NWs: (a) the cumulative normalized absorption profile $A(x, \lambda)$ showing different wavelengths being absorbed at various depths of the structure; (b) the cumulated normalized absorption for three separate bands of wavelengths. The shortest wavelength band (210−800 nm) is absorbed very quickly at smaller depths (x < 800 nm), which contain nanowires with relatively small diameter (~100 nm). The higher bands are absorbed relatively weakly within the first 800 nm and more strongly within the region with larger diameter nanowires (x > 800 nm).

namely, the depth specific wavelength-dependent absorption (see Figure 5). As we will show in the following discussion, the RBNW arrays have the ability to differentiate the three distinct regions for filtering and absorbing UV, Vis, and IR waves in the same structure. This effect arises from the geometry of the stacked NW and not from the electronic properties of the NWs.

To understand the wavelength-dependent absorption in various regions of the stacked NW, let us begin with a simple argument. If the individual branches of the RBNW array are approximated as isolated, noninteracting waveguides, then the cutoff wavelength ($\lambda_{cutoff}/n_{InSb}$) of the InSb waveguide is given by

$$\frac{\lambda_{cutoff}/n_{InSb}}{2} = d \qquad (2)$$

where d is the diameter of the NW. Assuming, the average refractive index of InSb n_{InSb} in the 300−1000 nm range is ~4.25,[19] the λ_{cutoff} for region 2 (d = 100 nm) is ~850 nm, while that of region 3 (d = 150 nm) is ~1275 nm. Incident wavelengths shorter than these cutoffs would efficiently couple to the nanowires and be absorbed within the respective region. Longer wavelengths would pass through the respective layers, with significantly reduced absorption and reflection. Note that the calculated cutoff for region 1 (d = 20 nm) is less than 300 nm, so the nanowires in this region are not expected to absorb significantly within the measured wavelength range. In short, the wavelength range absorbed within each region can be independently controlled by controlling the average diameter (and randomness) within the respective region. While such effects can be achieved by employing layers with different bandgaps or through electronic size quantization, the effect in this study arises from the structure itself, rather than the electronic properties of the material.

This elementary argument is supported by detailed numerical simulation result in Figure 5a (for RBNW2). The wavelength-resolved solution shows that nearly 95% of the coupled light with λ < 680 nm is absorbed by the top portion (~800 nm) of the BNW array. Only a small fraction of the longer wavelength photons are absorbed in this region. As we move deeper into the structure (region with d ~ 150 nm), the normalized absorbance exceeds 90% for λ < 1000 nm and approaches 80% for λ ~ 1000−1300 nm. If the NWs within each region were spatially uniform, sharp cutoff in the absorption spectra of UV, vis, and IR regions of the incident waves could be assigned to unique spatial regions. The gradual cutoff (linear decrease of absorption vs wavelength) in the absorption spectrum is caused by the randomness of the diameter distribution. Figure 5b shows a much simpler picture of this analysis. The normalized absorption is subdivided into three wavelength bands. As we see, λ ~ 201−800 nm rapidly reaches high normalized absorption (top 800 nm of the NW). The longer wavelengths are not strongly absorbed in the top 800 nm but are absorbed in the underlying region, containing larger diameter NWs (d ~ 150 nm). As noted earlier, the wavelength-dependent absorption does not arise from size quantization effects. Therefore, our tailored broadband absorption in UV−vis and the wavelength-dependent absorption in the IR region are attributed to structural effects.

An interesting corollary to the discussion above is that the observed absorbance and reflectance properties of such hierarchical structures cannot be reproduced by effective media approximation. Since photonic coupling effects are typically not included, wavelength-dependent absorption effects within the various regions are not accurately modeled using effective media. In order to achieve low reflectance, typical impedance matching approaches based on effective media approximations would employ a structure with a monotonic change in the volume fraction from air to the dielectric medium (InSb), corresponding to a gradual change in the refractive index. In the case of the RBNW arrays, the volume filling fractions inferred from SEM imaging (~19.6%, ~16.2%, and ~9.1% in the top, intermediate, and bottom regions, respectively) decrease with increasing depth, indicating that the lower reflectance compared to bulk InSb does not arise from this impedance matching. The low reflectance of our RBNW arrays compared to bulk InSb is attributed to the photonic coupling and random size distributions within the arrays.

In summary, we have developed hierarchical InSb RBNW arrays and measured the reflectance and absorbance spectra for these arrays. The nominal size distribution within each of the three regions has been determined by FESEM. The samples exhibit a very low broadband reflectance with near unity

dx.doi.org/10.1021/nl302803e | Nano Lett. 2012, 12, 6112−6118

normalized absorbance in UV−vis range and a wavelength selective absorbance in the NIR range. A model considering the diameter-dependent photonic coupling and random distribution of diameters has been used to analyze structures representing the various RBNW samples. The low reflectance and wavelength-dependent absorbance are both explained in terms of cutoff frequencies for photonic coupling into the nanowires in a given region (specific diameter). The randomness in the structure broadens the absorption spectra and can in principle be used to achieve tailored photonic properties, including specific absorbance profiles. This ability to tailor photonic properties through structure, both average diameters and randomness, could enable novel future optoelectronics devices, including wavelength-selective IR detectors/imagers and photovoltaic devices.

Methods. *Branched PAA Substrate.* Commercially available PAA membranes (Anodisc 13 from Whatman Co.) were used as the growth template for the randomly branched arrays. Near one surface of the PAA membrane (the "top"), randomly branched pores are observed, with average diameters varying from ∼20 nm near the surface to ∼150 nm at a depth of ∼1.5 μm. Throughout the remainder of the 60 μm thick membrane, the average pore diameter increases to ∼150 nm. Prior to electrodeposition, a 100 nm thick gold layer was e-beam evaporated onto the top surface of the PAA.

Deposition of InSb Nanowires. The nanowires were grown by electrodeposition of InSb in the branched PAA template in a three-terminal electrochemical cell employing the gold layer as cathode, platinum mesh as anode, and Ag/AgCl (in saturated NaCl) as the reference electrode. An aqueous solution containing indium chloride, antimony chloride, citric acid, and potassium citrate was used as electrolyte.[20] Prior to the deposition, the template was dipped into the electrolyte solution for 6−8 h. The overall electrochemical reaction at the cathode is

$$SbO^{+} + In^{3+} + 2H^{+} + 6e^{-} \rightarrow InSb + H_2O$$

The nanowire growth was performed using a deposition potential of −1.4 V vs the reference electrode. The length of the RBNWs array was controlled by monitoring the integrated current during the growth time. If N_M, z, and N_A denote the number of moles of material, atomic number, and Avogadro's number, respectively, then the total charge Q_{total} involved in the reaction is estimated as $Q_{total} = zN_AN_M$. The Q_{total} can be related to the deposition current, I, via $Q_{total} = \int I\,dt$. For a given Q_{total}, the average wire length was calculated using the bulk volume density of InSb and an estimate of the pore volume. Following growth and annealing, FESEM images were used to verify this estimate of average length. Following deposition, the samples were rinsed thoroughly in DI water and dried completely on a hot plate at 90 °C.

Optical Measurements. Prior to the optical measurements, the RBNW samples were thoroughly cleaned with ultrapure DI water, dried with N_2 gas, and prebaked at ∼90 °C to thoroughly dry. The gold electrode was etched away using gold etchant (from Transene Co.). For reflectance and transmittance measurements, a PerkinElmer UV−vis−NIR spectrophotometer (Model Lambda 950) with an integrating sphere arrangement was used. Prior to the each set of measurements, the system was calibrated with the white standard reflector from PerkinElmer. Also with identical experimental conditions, the reflectance and transmittance spectra of a blank BPAA were recorded, and the absorbance was found to be less than 1% for wavelengths larger than 850 nm (our spectrum of interest). After all instrumental calibration, data of RBNW1 and RBNW2 were taken.

■ ASSOCIATED CONTENT

Supporting Information

InSb nanowire growth, branched structure and crystal structure of the nanowires, statistical analysis of diameter of the middle and bottom stacks of InSb NWs in the branched nanowire array, numerical simulation of RBNWs array, and "absorbance" and "normalized absorbance". This material is available free of charge via the Internet at http://pubs.acs.org.

■ AUTHOR INFORMATION

Corresponding Author

*E-mail: alam@purdue.edu (M.A.A.); janes@ecn.purdue.edu (D.B.J.).

Author Contributions

‖These authors contributed equally.

Author Contributions

D.B.J. and M.A.A. designed the experiments. S.R.D. and A.M. had grown the nanowires; S.R.D. did the clean room fabrication processing, performed SEM of BNWs and single InSb nanowires, and characterized the material aspects. A.M. and S.R.D. performed the optical measurements, A.M. analyzed the optical data; M.R.K. did the COMSOL and MATLAB simulation for the structure. All authors have given approval to the final version of the manuscript.

Notes

The authors declare no competing financial interest.

■ ACKNOWLEDGMENTS

This work was supported by Center for Re-Defining Photovoltaic Efficiency through Molecule Scale Control, an Energy Frontier Research Center (EFRC) funded by the U.S. Department of Energy, Office of Science, Office of Basic Energy Sciences, under Award 2(ACCT5-64852) and by National Science Foundation under Grant ECCS-1202281. We thank Dr. D. Zakharov for assistance in HRTEM measurements and Prof. X. Ruan for providing his facility for optical measurements.

■ REFERENCES

(1) Joannopoulos, J. D.; Villeneuve, P. R.; Fan, S. *Nature* **1997**, *386*, 143−149.
(2) Shalaev, V. M. *Nat. Photonics* **2007**, *1*, 41−48.
(3) Hu, L.; Chen, G. *Nano Lett.* **2007**, *7*, 3249−3252.
(4) Zhang, A.; Kim, H.; Cheng, J.; Lo, Y.-H. *Nano Lett.* **2010**, *10*, 2117−2120.
(5) Seo, K.; Wober, M.; Steinvurzel, P.; Schonbrun, E.; Dan, Y.; Ellenbogen, T.; Crozier, K. B. *Nano Lett.* **2011**, *11*, 1851−1856.
(6) Kayes, B. M.; Atwater, H. A.; Lewis, N. S. *J. Appl. Phys.* **2005**, *97*, 114302.
(7) Zhao, X.; Wei, C. M.; Yang, L.; Chou, M. Y. *Phys. Rev. Lett.* **2004**, *92*, 236805.
(8) Fan, Z.; Kapadia, R.; Leu, P. W.; Zhang, X.; Chueh, Y.-L.; Takei, K.; Yu, K.; Jamshidi, A.; Rathore, A. A.; Ruebusch, D. J.; Wu, M.; Javey, A. *Nano Lett.* **2010**, *10*, 3823−3827.
(9) Chueh, Y.-L.; Fan, Z.; Takei, K.; Ko, H.; Kapadia, R.; Rathore, A. A.; Miller, N.; Yu, K.; Wu, M.; Haller, E. E.; Javey, A. *Nano Lett.* **2009**, *10*, 520−523.
(10) Xiong, Z.; Zhao, F.; Yang, J.; Hu, X. *Appl. Phys. Lett.* **2010**, *96*, 181903.
(11) Bao, H.; Ruan, X. *Opt. Lett.* **2010**, *35*, 3378−3380.

(12) Muskens, O. L.; Rivas, J. G.; Algra, R. E.; Bakkers, E. P. A. M.; Lagendijk, A. *Nano Lett.* **2008**, *8*, 2638−2642.
(13) Street, R. A.; Wong, W. S.; Paulson, C. *Nano Lett.* **2009**, *9*, 3494−3497.
(14) Pignalosa, P.; Lee, H.; Qiao, L.; Tseng, M.; Yi, Y. *AIP Adv.* **2011**, *1*, 032124.
(15) Schuurmans, P. F. J.; Vanmaekelbergh, D.; van de Lagemaat, J.; Lagendijk, A. *Science* **1999**, *284*, 141−143.
(16) Levi, L.; Rechtsman, M.; Freedman, B.; Schwartz, T.; Manela, O.; Segev, M. *Science* **2011**, *332*, 1541−1544.
(17) Garnett, J. C. M. *Philos. Trans. R. Soc. London, A* **1904**, *203*, 385−420.
(18) Multiphysics Modeling and Simulation Software: http://www.comsol.com/ http://www.comsol.com/ (accessed July 9, 2012).
(19) Refractive index database: http://www.filmetrics.com/refractive-index-database.
(20) Zhang, X.; Hao, Y.; Meng, G.; Zhang, L. *J. Electrochem. Soc.* **2005**, *152*, C664−C668.